

PHASE CONTROL IN THE MASS-SPRING MODEL WITH NON-SMOOTH STIFFNESS AND EXTERNAL EXCITATION

MATTIA COCCOLO

*Nonlinear Dynamics, Chaos and Complex Systems Group, Departamento de Física
Universidad Rey Juan Carlos, Tulipán s/n, 28933 Móstoles, Madrid, Spain*

JESÚS M. SEOANE

*Nonlinear Dynamics, Chaos and Complex Systems Group, Departamento de Física
Universidad Rey Juan Carlos, Tulipán s/n, 28933 Móstoles, Madrid, Spain*

GRZEGORZ LITAK

*Department of Applied Mechanics, Lublin University of Technology,
Nadbystrzycka 36, PL-20-618 Lublin, Poland*

MIGUEL A.F. SANJUÁN

*Nonlinear Dynamics, Chaos and Complex Systems Group, Departamento de Física
Universidad Rey Juan Carlos, Tulipán s/n, 28933 Móstoles, Madrid, Spain*

Received (to be inserted by publisher)

The control of the chaotic dynamics in a nonlinear mass-spring model with non-smooth stiffness is analyzed here. This is carried out by applying the phase control technique, which uses a periodic perturbation of a suitable phase ϕ . For this purpose, we take as prototype model a system consisting in a double-well potential with an additional spring component, which acts into the system only for large enough displacements. The crucial role of the phase is evidenced by using numerical simulations and also by using analytical methods, such as the Melnikov analysis. We expect that our results might be fruitful and with implications in some mechanical problems such as suspension of vehicles, among others, where similar models are extensively used.

Keywords: Phase control, nonlinear oscillations, Melnikov criterion, chaos, non-smooth dynamical systems.

1. Introduction

There is a rich literature on chaotic systems either modeled by a set of nonlinear ordinary differential equations or with smooth functions of the displacement or the velocity [Spratt, 2003]. Non-smooth systems are very common in Engineering [Radons & Neugebauer, 2004; Litak *et al.*, 2007; Pavlovskaja & Wiercigroch, 2007] in which they have relevant implications. In the present paper we implement a control scheme to control the dynamics of the two stage mass-spring oscillator as shown in Fig. 1.

In this system the two considered springs are connected in a parallel way. One of them has nonlinear characteristics producing the double-well potential while the other one is acting according to the Hooke's law, $F = -kx$, as shown in Fig. 1. Such connections of springs are often considered in practical situations as

in the suspension of vehicles [Verros *et al.*, 2000; Von Wagner, 2004], among others. The effect of the linear spring on the two exterior nonlinear springs has been thoroughly analyzed by Litak *et al.* in Ref. [Litak *et al.*, 2012]. In this paper we focus our research in a suitable control implementation technique in order to obtain a desirable dynamical behavior.

Since the pioneering work on controlling chaos due to Ott, Grebogi and Yorke, [Ott *et al.*, 1990], different control schemes have been proposed that allow to obtain a desired response for a dynamical system by applying some small but accurately chosen perturbations. In this context, some techniques that allow avoiding escapes in open dynamical systems presenting transient chaos have been proposed, with applications to many different situations in physics and engineering (see Ref. [Aguirre *et al.*, 2004] and references therein). However, most of these methods are *feedback* methods, i.e., they require the application of a fast and adequate state-dependent perturbation to the system, so that in some experimental situations they might become unpractical.

In those situations it has been shown that sometimes applying a small and state-independent harmonic perturbation can lead to analogous results [Lima & Pettini, 1985; Meucci *et al.*, 1994]. The methods based on this idea are traditionally known as nonfeedback methods [Qu *et al.*, 1994]. Among them the phase control scheme [Qu *et al.*, 1994; Zambrano *et al.*, 2006,b; Litak *et al.*, 2007] has been found to be useful to control different behaviors in periodically driven dynamical systems, including not only control of a chaotic trajectory, but also other paradigmatic dynamical behaviors such as crisis-induced intermittency, control of escapes in open dynamical systems [Seoane *et al.*, 2008], control of dynamics in excitable systems [Zambrano *et al.*, 2008], to cite just a few. This method focus on the role of the phase difference of a periodic perturbation with respect to the main forcing, which is adequately “tuned” in search of a desired response from the system. Another control method [Kapitaniak & Brindley, 1988], though based in a feedback procedure, was used to preserve transient chaos. In this last paper, the authors focused in the transient chaos and its lifetime using Lyapunov exponents.

Our aim in this paper is to show that the phase control method can be applied to non-smooth systems, which are used to model many systems in engineering.

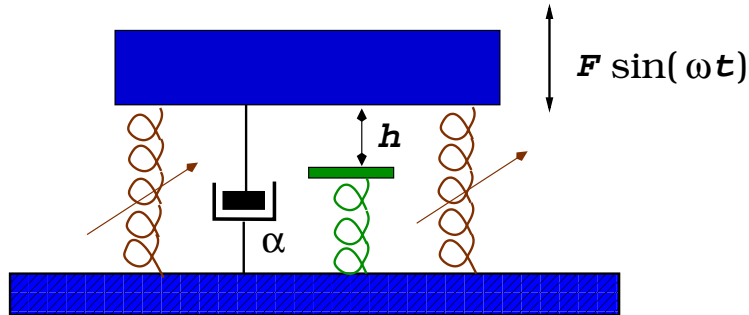


Fig. 1. Schematic plot of the two stage spring-mass model. The effective exterior springs in the figure are assumed to have the nonlinear characteristics, while the interior which introduces the non-smoothness, has a linear characteristics. h denotes the tip position of the spring free length with respect to the equilibrium point $x = 0$.

This paper is organized as follows. Section 2 presents a description of our model and the phase control scheme implementation. In section 3 we solve the corresponding differential equations and discuss the results explaining the role of the phase in the control of the dynamics. On the other hand, the numerical estimation of the integral can be done numerically. This concept, used in previous works [Litak *et al.*, 2008], is used in Sec. 4. After presenting the numerical results, confirming the estimated critical parameters, the paper ends with the conclusions and a discussion presented in Sec. 5.

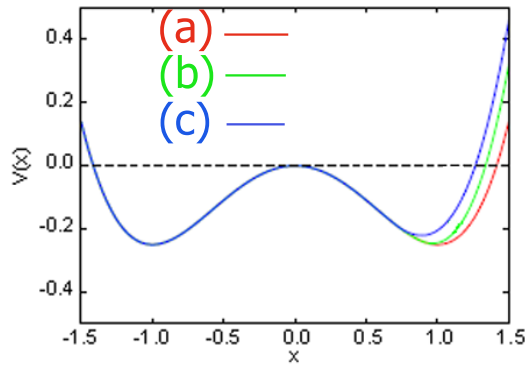


Fig. 2. (Color online) The solid curve represents the double-well symmetric potential $V_1(x) = -\frac{x^2}{2} + \frac{x^4}{4}$ and the potential obtained when the additional spring $V(x) = -\frac{x^2}{2} + \frac{x^4}{4} + k\frac{(x-x_0-h')^2\Theta(x-x_0-h')}{2}$, for $k = 1$ is considered. The parameters $x_0 + h' = h$, $x_0 = 1$ is the position of the right hand side stable equilibrium point, while h' ($h' = 0$ for (a); -0.1 for (b); and -0.3 for (c)) denotes the tip position of the spring free length.

2. Model description

The model we take as prototype, according to Fig. 1, is given by the non-dimensional equation of motion [Litak *et al.*, 2012]:

$$\ddot{x} + \alpha\dot{x} - x + x^3 + k(x-h)\Theta(x-h) = F\sin(\omega t), \quad (1)$$

where α is the damping parameter and k is a constant associated to the linear spring of a certain length and a non-symmetrical contact loss. $\Theta(x)$ is the Heaviside step function, F is the amplitude of a harmonic excitation with frequency ω and h is the constant corresponding to the position of the spring free length tip with respect to the equilibrium point $x = 0$ (see Fig. 1). We can observe that if $k = 0$ we have the well known Duffing oscillator [Duffing, 1918; Aguirre & Sanjuán, 2000; Baltanás *et al.*, 2001].

The restoring force $F(x)$ is defined by the potential $V(x)$ (Fig. 2) as follows

$$F(x) = -\frac{\partial V}{\partial x} = x - x^3 - k(x-h)\Theta(x-h), \quad (2)$$

$$V(x) = -\frac{x^2}{2} + \frac{x^4}{4} + \frac{k(x-h)^2\Theta(x-h)}{2}, \quad (3)$$

where we have taken $x_0 + h' = h$ with $x_0 = 1$ and $h' = -0.1$.

In Fig. 2, we clearly observe the asymmetry induced by the additional linear spring with clearance (curves (b) and (c)) with respect to the smooth restoring force case (curve (a)). Notice that the solid red curve represents the symmetric double well potential.

In order to understand better the behavior of our system, we show numerical plots of both, trajectories in phase space and Poincaré sections. For this purpose, we have taken the following values of the parameters: $\alpha = 0.15$, $\omega = 1$ and $F = 0.258$. Figures 3(a) and 3(a') represent both the typical chaotic trajectory and the typical Poincaré section of the Duffing oscillator for the smooth case. Furthermore, we can see in Fig. 4 the bifurcation diagram of the x variable as a function of the forcing amplitude F , and we can see that $F = 0.258$ is well into the chaotic region.

Figures 3(b) and 3(b') show the same kind of plots for the non-smooth case for $k = 0.2$ and $h = 0.3$. We can observe, in the right side (region in which $x > 0$) of Fig. 3(a') and Fig. 3(b'), the effect of the non-smooth term. Provided that the profile of the right well of the Duffing oscillator becomes steeper due to the non-smooth term, we can see how both the right side of the trajectories and the attractor are slightly compressed compared to the unperturbed case (Fig. 2).

In order to control the dynamics of this system we implement the phase control technique by adding a external perturbation in the form $\varepsilon\sin(r\omega t + \phi)$, where $\varepsilon \ll F$ is the amplitude of the control, r a positive constant, and ϕ the phase difference between the main driving and the control term. From now on we call

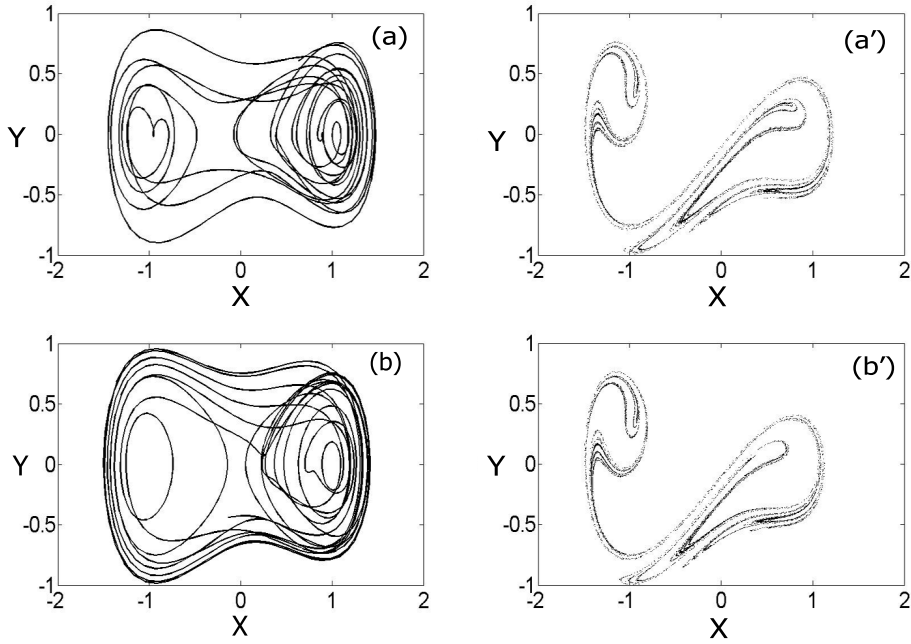


Fig. 3. Numerical plots of both, phase portraits ($x, y = \dot{x}$) (Fig. a and Fig. b) and corresponding Poincaré sections (Fig. a' and Fig. b'), for the Duffing oscillator case and for the non-smooth case with parameter values $\alpha = 0.15$, $F = 0.258$, $k = 0.2$ and $h = 0.3$, respectively [Litak *et al.*, 2012]. We observe the effect of the non-smooth term on the right side of the pictures: in presence of non-smoothness, both the trajectories and the attractor look similar to the unperturbed ones, but their right side is slightly compressed.

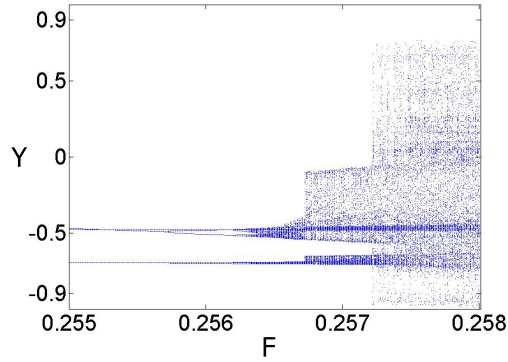


Fig. 4. Numerical bifurcation diagram ($y = \dot{x}$ versus F) of the Duffing oscillator in absence of the linear spring with clearance ($\alpha = 0.15$, $k = 0.2$, $h = 0.3$). We observe periodic regions and chaotic regions depending of the value of F . The onset of chaos takes place at $F \simeq 0.257$.

it simply *phase* and it will be the main parameter of our control method. Once we introduce our control scheme, the equation of motion of our system can be written as:

$$\ddot{x} + \alpha \dot{x} - x + x^3 + k(x - h)\Theta(x - h) + \varepsilon \sin(r\omega t + \phi) = F \sin(\omega t), \quad (4)$$

Since we are working in the context of a mechanical device, the control term $\varepsilon \sin(r\omega t + \phi)$ is quite natural and very easy to implement experimentally.

3. Melnikov analysis

Here we provide, by using Melnikov analysis, theoretical arguments in order to show the different parameter regions in which the system is in a chaotic regime or in a periodic regime and how the control scheme acts on the dynamics of the system. The regions of transient and permanent chaos can be predicted by using the perturbative Melnikov analysis [Moon & Li, 1985; Baltanás *et al.*, 2002; Almendral *et al.*, 2004].

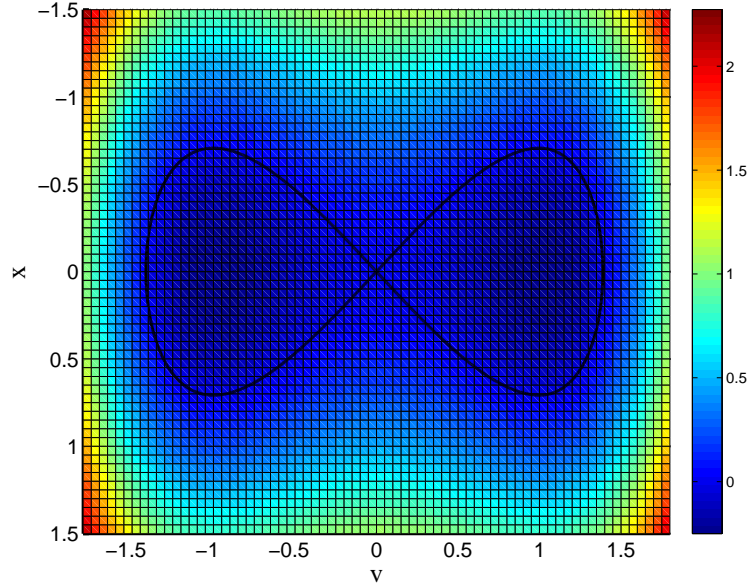


Fig. 5. (Color online) Homoclinic orbits of the corresponding unperturbed Hamiltonian in the phase plane $(x, v = \dot{x})$.

According to the Melnikov analysis we assume that the force and the damping parameter can be treated as perturbations, so that we can rewrite:

$$F \sin(\omega t) + \delta F \sin(r\omega t + \phi) \rightarrow \epsilon \tilde{F}(\sin(\omega t) - \delta \sin(r\omega t + \phi)), \quad \alpha \rightarrow \epsilon \tilde{\alpha}. \quad (5)$$

Consequently, the equations of the system can be written as:

$$\dot{x} = v, \quad (6)$$

$$\dot{v} = x - x^3 - k(x - h)\Theta(x - h) = \epsilon(-\tilde{\alpha}\dot{x} + \tilde{F}(\sin(\omega t) - \delta \sin(r\omega t + \phi))). \quad (7)$$

Thus, the unperturbed Hamiltonian, i. e., in absence of both forcing and damping, reads:

$$H_0 = \frac{v^2}{2} - \frac{x^2}{2} + \frac{x^4}{4} + k \frac{(x - h)^2 \Theta(x - h)}{2}. \quad (8)$$

The homoclinic orbits needed for the Melnikov method are obtained by integrating out the following expression:

$$\frac{dt}{dx} = \frac{1}{v} = \frac{1}{\sqrt{2V(x)}}. \quad (9)$$

Thus, we obtain:

$$t - t_0 = \frac{1}{\sqrt{x^2 - \frac{x^4}{2} - k(x - h)^2 \Theta(x - h)}}. \quad (10)$$

In case of the typical double-well potential and for the right hand side half-plane $x < 0$, we can easily integrate the above expression to the analytic formula:

$$x^*(t) = \pm \frac{\sqrt{2}}{\cosh(t - t_0)}, \quad v^*(t) = \pm \frac{\sqrt{2} \tanh(t - t_0)}{\cosh(t - t_0)}. \quad (11)$$

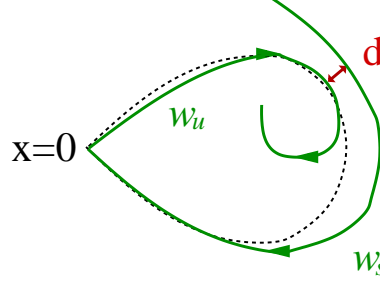


Fig. 6. A schematic picture of unperturbed (plotted with a dotted line) and perturbed homoclinic orbits (stable W_s and unstable W_u manifolds plotted with full lines). The distance between W_s and W_u is d . And $x = 0$ indicates the location of the saddle point.

The unperturbed Hamiltonian and the the homoclinic orbits are presented in Fig. 3.

After adding perturbations, the homoclinic orbits split to the stable and unstable manifolds, denoted by W_s and W_u , respectively. The existence of cross-sections between W_s and W_u manifolds signals the Smale horseshoe scenario of transition to chaos (see Fig. 3). Consequently, the distance d between the invariant manifolds can be estimated in terms of the Melnikov function since $d \sim M(t_0)$:

$$M(t_0) = \int_{-\infty}^{\infty} h_0(x^*, v^*) \wedge h_1(x^*, v^*) dt, \quad (12)$$

where \wedge defines the wedge product ($dx \wedge dv = -dx \wedge dv$, $dx \wedge dx = dv \wedge dv = 0$). The corresponding differential forms h_0 means the gradient of the unperturbed Hamiltonian

$$h_0 = (-x^* + (x^*)^3 + (x - h)\Theta(x^* - h))dx + v^*dv, \quad (13)$$

while h_1 is a perturbed Hamiltonian

$$h_1 = (\tilde{F}(\sin(\omega t) - \delta \sin(r\omega t + \phi))) - \tilde{\alpha}v^*)dx. \quad (14)$$

It is important that all differential forms in the above expressions are defined on the homoclinic orbits $(x, v) = (x^*, v^*)$. Thus, the Melnikov function $M(t_0)$ reads:

$$M(t_0) = \int_{-\infty}^{\infty} v^*(\tilde{F}(\sin(\omega t) - \delta \sin(r\omega t + \phi))\tilde{\alpha}v^*)dt. \quad (15)$$

A condition for a global homoclinic transition, corresponding to a horseshoe type, can be written as:

$$\bigvee_{t_0} M(t_0) = 0 \quad \text{and} \quad \frac{\partial M(t_0)}{\partial t_0} \neq 0. \quad (16)$$

The above condition is valid [Guckenheimer & Holmes, 1983] for smooth potentials belonging to the C^2 class ($V \in C^2$).

On the other hand, for the nonsmooth case, for $k \neq 0$ (Figs. 2 and 5), the analytic treatment is difficult, but the corresponding Melnikov criterion (Eqs. 11-15) could be found numerically [Litak *et al.*, 2012]. Note that in this situation the potential is not smooth enough as it belongs to the C^1 class functions. Thus, according to Kunze and Küpper [2001] there would be corrections related to the singular points associated to the non-smoothness $x = h$. However, the above corrections are more important for a precise estimation of the homoclinic bifurcation. In our case, we solve the integral numerically, and our approximation will include Kunze and Küpper corrections [2001] within the integration error. It should be noted that we give corrections, in some sense, by averaging the integral kernel for different limits $x \rightarrow h$.

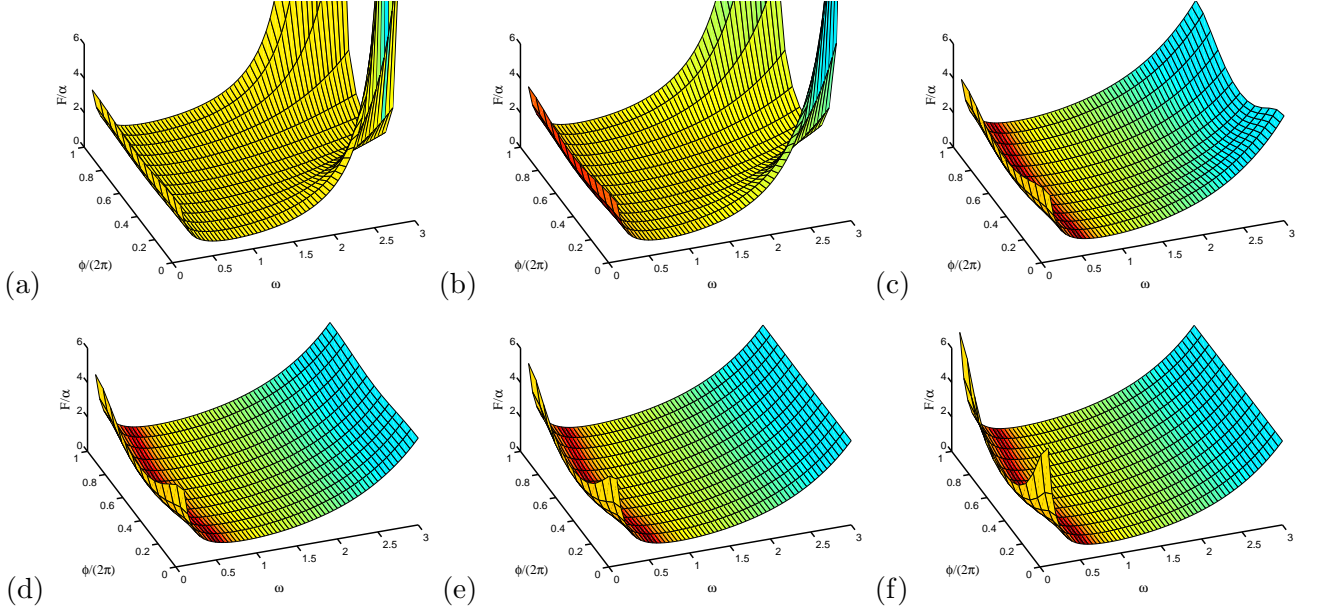


Fig. 7. (Color online) The numerically estimated critical surfaces $\eta = F/\alpha$ versus ω that separate the regular (below the curves) and chaotic (above the curves) parameter regions for $k = 1$ and $h = 1.0$. The control phase ϕ was chosen as $\phi = 1/4, 1/3, 1/2, 1, 2, 3$ for (a),(b), ..., and (f) (respectively).

Finally, from Eqs. 14 and 15, the critical region of the ratio $\eta = \tilde{F}/\tilde{\alpha} = F/\alpha$ as a function of ω can be estimated as

$$\eta(\omega) = \min|I_1/I_2(\omega)|, \quad (17)$$

where the integrals I_1 and I_2 have the following forms

$$I_1 = \int_{-\infty}^{\infty} (v^*(t))^2 dt \quad \text{and} \quad I_2 = \int_{-\infty}^{\infty} v^*(t)(\sin(\omega(t+t_0)) - \delta \sin(r\omega(t+t_0) + \phi)) dt \quad (18)$$

The condition for the second potential well on the left hand side in Fig. 2 with a smooth heteroclinic orbit (Fig. 5) can be expressed analytically as for the case $k = 0$. Introducing $v^*(t)$ into Eq. 17 [Holmes, 1979; Guckenheimer & Holmes, 1983] we integrate:

$$I_1 = \frac{4}{3}, \quad I_2 = \frac{\sqrt{2}\pi\omega}{\cosh(\pi\omega/2)} \sin(\omega t_0) - \delta \frac{\sqrt{2}\pi r\omega}{\cosh(\pi r\omega/2)} \sin(r\omega t_0 + \phi). \quad (19)$$

For $r = 1$ the above formula can be easily simplified by choosing the free integration parameter t_0 in such a way that $\max|\sin(\omega t_0 + \alpha)| = 1$ (where $\sin \alpha = -\delta \sin \phi / \sqrt{1 + \delta^2 - 2\delta \cos \phi}$).

Thus I_2 can be written as

$$(I_2)_{max} = \frac{\sqrt{2}\pi\omega}{\cosh(\pi\omega/2)} \sqrt{1 + \delta^2 - 2\delta \cos \phi}. \quad (20)$$

Finally, for the condition for the left side potential well (Fig. 2), $\eta(\omega)$ (Eq. 16) could be expressed analytically as

$$\eta(\omega) = \frac{2\sqrt{2}}{3\pi\omega\sqrt{1 + \delta^2 - 2\delta \cos \phi}} \cosh(\pi\omega/2). \quad (21)$$

The condition for the right hand side potential well (nonsmooth case) in Fig. 2 (for $k = 0.450$, $h = 1$) has been computed numerically. By changing the h we could see the effect of an additional spring on the dynamics (Fig. 1). The results of the Melnikov analysis are presented in Fig. 7.

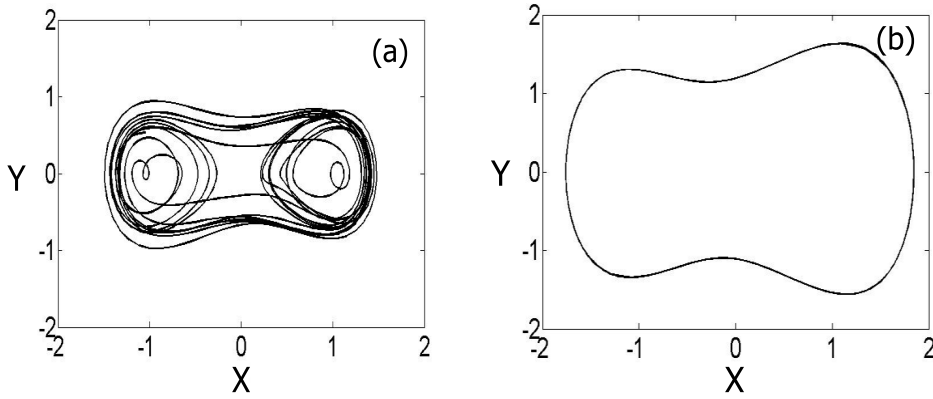


Fig. 8. Numerical plots trajectories in the phase plane ($x, y = \dot{x}$) of the system without control (Fig. a) and with control (Fig. b). Parameter values are: $k = 0.45$, $h = 1$, $F = 0.258$ and the control parameters are $\varepsilon = 0.1$ and $\phi = \pi$. We observe the clear influence of the phase to control the dynamics of our system.

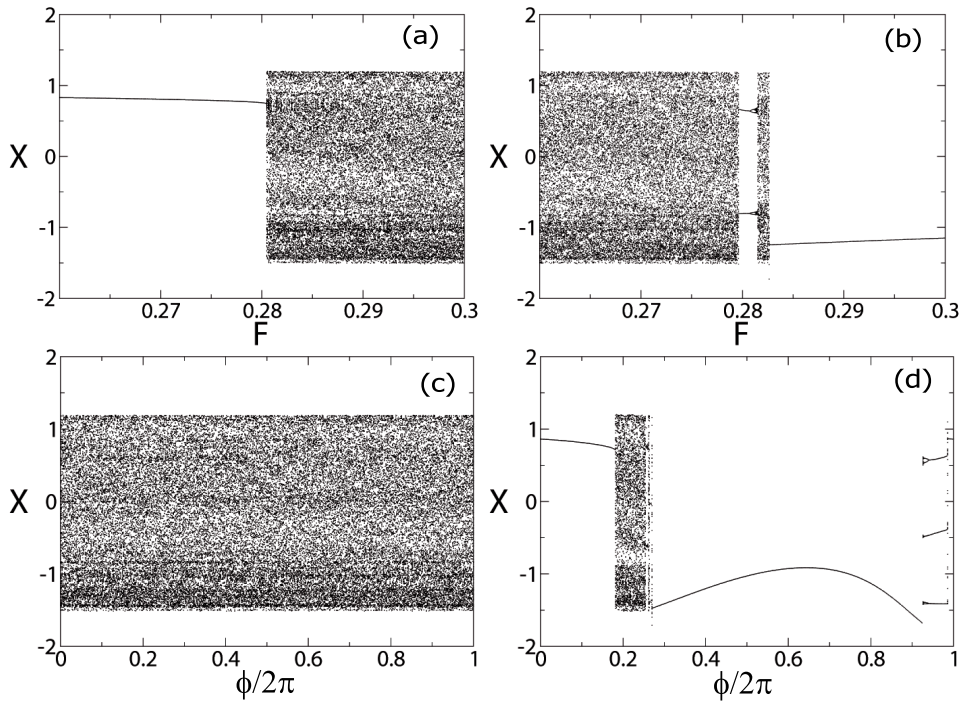


Fig. 9. Numerical bifurcation diagrams of the variable x versus F ((a) and (b)) for $k = 0.45$ and $h = 1$ (a) without control (b) with control parameters: $\varepsilon = 0.2$, $\phi = \pi$. Numerical bifurcation diagrams of the variable x versus $\phi/2\pi$ ((c) and (d)). (c) $F = 0.3$ without control and (d) $F = 0.3$ with control parameters $\varepsilon = 0.2$ and $\phi = \pi$.

4. Numerical simulations

We have carried out some numerical simulations showing a very good agreement with the analytical results shown previously. We have simulated the mathematical model by using a 4th order Runge-Kutta integration scheme [Burden & Faires, 1997]. Trajectories in phase space in both cases without control and with control are presented in Fig. 8. Figures 8(a) and 8(a') show a chaotic trajectory for $h = 1$ and $k = 0.2$. If we increase the value of k , say $k = 0.7$, the influence of the linear spring becomes relevant since the chaotic motion disappears and it becomes periodic falling into an attractor, as shown in Fig. 8(b'). It seems then that there is a critical value of k for which a periodic attractor close to the right well of the system appears, making the orbits become periodic.

Figures 9(a) and 9(b) provide a deeper insight on this phenomenon. In Fig. 9(a), a bifurcation diagram

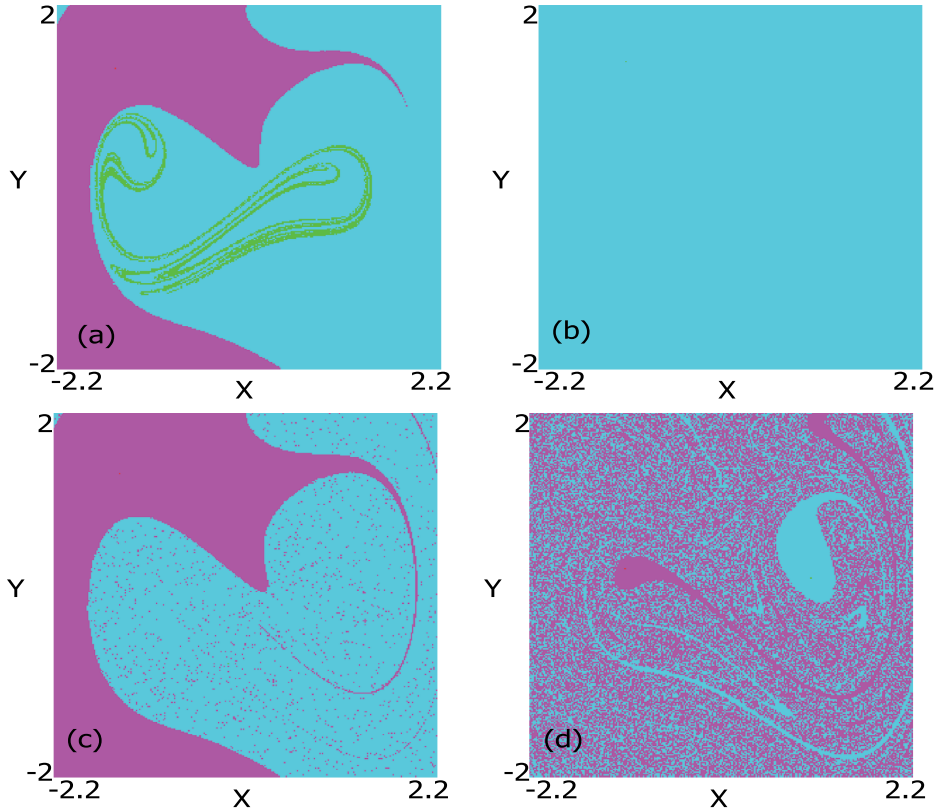


Fig. 10. (Color online) Plots of the basins of attraction of our system (in the phase plane $(x, y = \dot{x})$) for (a) $F = 0.3$, $k = 0.45$ and $h = 0.1$ without control in which chaotic motions take place, (b) $F = 0.26$, $k = 0.45$ and $h = 0.1$ in which the regular motions take place. (c) and (d) with control ($\varepsilon = 0.2$) (c) $\phi = \pi$ and (d) $\phi = 0$. Finally, we observe the important influence of the phase since the basin structure is altered by the phase effects.

of the system of x versus F with non-smoothness parameters $k = 0.45$ and $h = 1$, we can see that for small forcing the system displays periodic behaviour, since the linear spring induces a regular behavior into the system. But as F is increased, chaos arises in what seems to be an inverse saddle-node bifurcation. Saddle-node bifurcations are widespread in dynamical systems, for example it is the bifurcation that gives rise to the period-three window in the logistic map [Robinson, 2004]. In Fig. 9(b), we show the bifurcation diagram of the variable x versus k for $h = 1$ and $F = 0.258$. We see that the system is chaotic until the value of k is too large and a periodic attractor arises in the right well, so the pre-existing chaotic attractor disappears through a saddle-node bifurcation. An energetic interpretation can be provided for this phenomenon: when adding the non-smooth stiffness, the system does not change drastically its behaviour until k is sufficiently large, when an attractor arises that stabilizes the orbit. After this, the system can be driven again to the chaotic state by increasing the forcing amplitude F .

The bifurcation diagrams of x versus ϕ shown in Figs. 9(c) and 9(d) for $k = 0.45$, $k = 1$, $h = 1$, respectively, for the uncontrolled case (Fig. 9(c)) and for the control case with $\varepsilon = 0.2$ and $r = 1$. We clearly observe the strong influence of the phase in the taming of the dynamical behavior of our system. Values of phase ϕ induce both chaotic behavior with possible coexistence of several attractors and regular motions according to Fig. 4(d).

In order to have a better understanding of these results we have plotted the basins of attraction for different situations.

Figures 10(a) and (b) represent, for $\alpha = 0.15$, $\omega = 1$, $h = 0.1$ and $k = 0.45$, the typical basin of attraction of the Duffing system [Aguirre & Sanjuán, 2000; Aguirre *et al.*, 2009] in presence of the linear spring without control for $F = 0.26$ and $F = 0.3$, respectively. We observe the effect of the forcing in the sense that we can observe a transition from a chaotic regime (Figure 10(a)) to a non-chaotic regime (Figure 10(b)) insofar we increase the value of the forcing amplitude. The chaotic attractor (denoted in

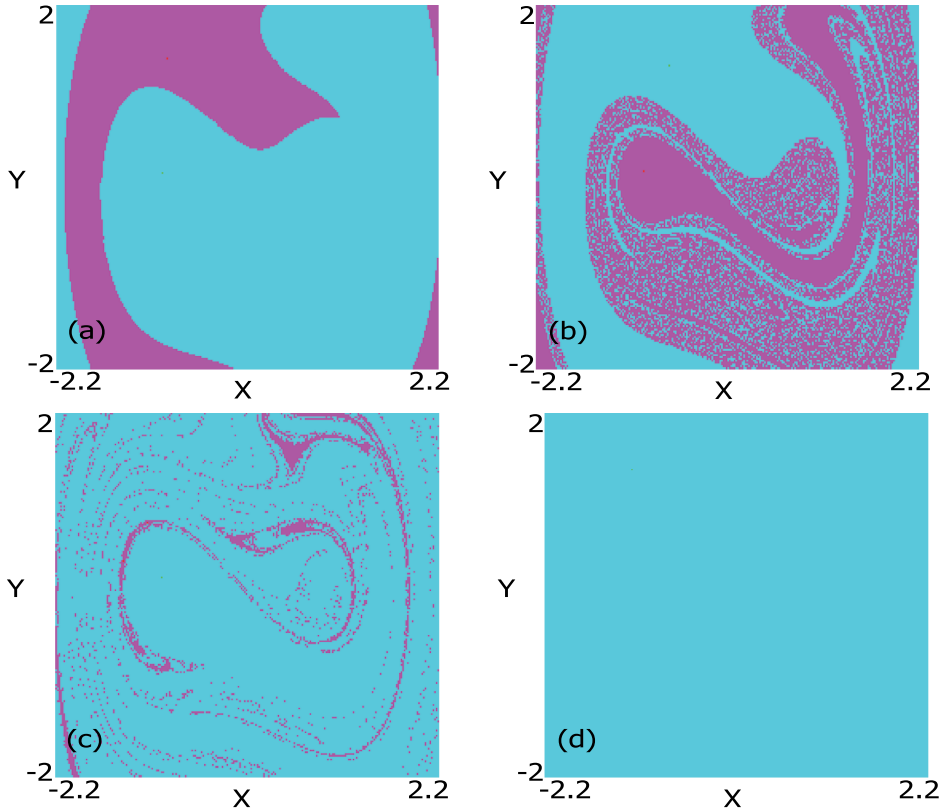


Fig. 11. (Color online) Plots of the basins of attraction of our system (in the phase plane $(x, y = \dot{x})$) for $r = 1/2$, $\varepsilon = 0.2$, (a) $\phi = 0$, $F = 0.26$, $k = 0.45$ and $h = 0.1$ in which regular motions take place, (b) $\phi = 0$, $F = 0.30$, $k = 0.45$ and $h = 0.1$ in which the topology is rather complicated since the boundaries of the basins are fractal. (c) and (d) with $\phi = \pi$. Finally, we observe the effects of the phase since the boundaries can be fractal or a complete predictable scenario can appear.

green color) is destroyed and the motions become regular as clearly shown in the bifurcation diagram in Fig. 4(b).

We have also analyzed numerically the effects of control on the dynamics of the system for different values of the frequency.

Figures 10(c) and (d) show, in presence of control $\varepsilon = 0.2$ and $F = 0.26$, the effect of the phase ϕ in the case of resonant frequencies, $r = 1$, between the main driving and the control term. We easily observe the importance of the phase in both the dynamics and the topology of the system. The chaotic attractor is smeared as we can see Fig. 10(c) when $\phi = \pi$. On the other hand, the existence of multiple attractors takes place for the value $\phi = 0$ as depicted in Fig. 10(d). In this last case, the topology of phase space is quite complicated and the basins possess the Wada property [Aguirre *et al.*, 2009] and the system becomes unpredictable.

In order to provide more evidence of the phase control scheme, in both the dynamics and the topology of the system, we have also considered its effects for the cases of non-resonant frequencies, $r \neq 1$.

Figures 11(a-d) show, the basins of attraction for the case $r = 1/2$ and $\varepsilon = 0.2$. The other parameters are fixed as follows: $k = 0.45$, $\mu = 0.15$, $\omega = 1$ and $h = 0.1$. Figures 11(a) and (b) represent the case of $\phi = 0$ and $E = 0.26$ and $E = 0.3$, respectively. Figure 11(a) shows the existence of regular and periodic motions in which the system is completely predictable and the boundaries between the basins are smooth. In contrast, in Fig. 11(b) the topology is completely different. The boundaries between the basins are fractal and the system becomes unpredictable in several regions of phase space. On the other hand, Figs. 11(c) and (d) represent the case of $\phi = \pi$ and $E = 0.26$ and $E = 0.3$, respectively. The role of the phase ϕ is quite relevant since the structure of phase space is completely different as in the case in which $\phi = 0$. Figure 11(c) represents the erosion of one of the basins in which we can observe small regions in phase space in which the dynamics of the system is unpredictable. Insofar we increase the value of the energy, say

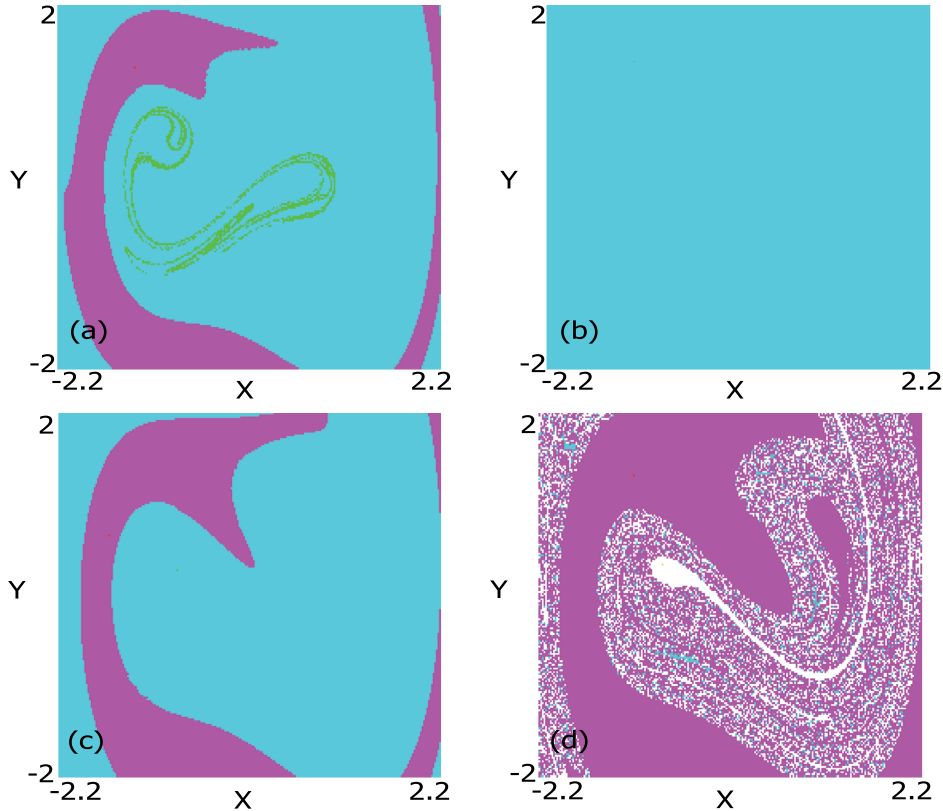


Fig. 12. (Color online) Plots of the basins of attraction of our system (in the phase plane $(x, y = \dot{x})$) for $r = 2$, $\varepsilon = 0.2$, (a) $\phi = 0$, $F = 0.26$, $k = 0.45$ and $h = 0.1$ in which chaotic motions take place and where we can observe the chaotic attractor denoted in green color, (b) $\phi = 0$, $F = 0.30$, $k = 0.45$ and $h = 0.1$ in which the topology is very simple since all motions are regular or periodic. (c) and (d) with $\phi = \pi$. Finally, we clearly see the relevant effects of the phase since the boundaries can be smooth with a complete predictable scenario from a dynamical point of view or phase space can have fractal structure, respectively.

$E = 0.3$ (see Fig. 11(d)), the phase space has one single attractor and all orbits are regular and periodic. These numerical results are in complete agreement with the Melnikov analysis shown in Figs. 7(b).

In the last part of this section, we analyze the influence of a non resonant situation, that is, $r = 2$. Figures 12(a-d) show the basins of attraction for the case $r = 2$ and $\varepsilon = 0.2$. The other parameters are fixed as follows: $k = 0.45$, $\mu = 0.15$, $\omega = 1$ and $h = 0.1$.

The existence of a chaotic attractor in Fig. 12(a) is clearly modified for the value $\phi = 0$ (see Fig. 12(b)) when we change the forcing amplitude from $F = 0.26$ to $F = 0.3$, where all orbits are periodic or regular according to Fig. 12(c). On the other hand, regular motions take place for the value $\phi = \pi$ and $F = 0.26$, becoming the system completely predictable according to its smooth boundaries. However, for $F = 0.3$, the phase space topology is rather complicated possessing fractal structures and multiple attractors for which the prediction is quite difficult, as shown in Fig. 12(d).

It should be also noted that the Melnikov criterion indicates rather the appearance of both the basin boundary destruction and also chaotic motion. This effect can be visible in Figs. 10, where the basins of attraction for three values in the vicinity of critical conditions that corroborate the results presented in Fig. 7 are shown. The different surfaces represent the existence of chaotic or regular motions for different values of the phase ϕ which are also in complete agreement with the numerical results presented in this section.

5. Conclusions and discussion

Our results show that the non-smooth systems can be controlled by using the phase control technique. For that purpose, we propose to rely on the numerical integration of the Melnikov integral in which we present

results on the effects of the phase difference between the main driving and the control.

The numerical bifurcation diagrams elucidate us clearly the role of F , k and ω for which the onset of the chaotic motions takes place and their control through the phase difference between both signals. Besides, by analyzing the different numerical bifurcation diagrams we conjecture both, the appearance and destruction of different attractors. This last result is corroborated by analyzing the evolution of the basin of attraction for different values of η . The basins of attraction show the creation and destruction of the different attractors for values of η close to the critical points where the dynamics changes from periodic to chaotic or viceversa.

Finally, we think that these results obtained in non-smooth systems including the clearance and dry friction phenomena to have important and relevant implications in problems of control in Engineering [Radons & Neugebauer, 2004].

Acknowledgement

We would like to thank Juan C. Vallejo for the fruitful discussions we have had during the development of this work. The basins of attraction (Figs. 10, 11 and 12) have been made using the software DYNAMICS [Nusse & Yorke, 1997]. This work was supported by the Spanish Ministry of Science and Innovation under project number FIS2009-09898. JS acknowledges warm hospitality received at Lublin University of Technology where part of this work was carried out. This paper has been partially supported by the Polish National Science Center (GL) under the grant agreement 2012/05/B/ST8/00080.

References

- Aguirre, J. & Sanjuán, M.A.F. [2002] “Unpredictable behavior in the Duffing oscillator: Wada basins,” *Physica D* **171**, 41–51.
- Aguirre, J., Viana, R. L. & Sanjuán, M.A.F. [2009] “Fractal Structures in Nonlinear Dynamics,” *Rev. Mod. Phys.* **81**, 333–386
- Aguirre J., d’Ovidio F. & Sanjuán M. A. F. [2004] “Controlling chaotic transients: Yorke’s Game of Survival” *Phys. Rev. E* **69**, 016203.
- Almendral, J.A., Seoane, J.M. & Sanjuán, M.A.F. [2004] “Nonlinear dynamics of the Helmholtz oscillator,” *Recent Res. Dev. Sound Vib.* **2**, 115–150.
- Baltanás, J.P., Trueba J.L. & Sanjuán M.A.F. [2002] “Nonlinearly damped oscillators,” *Recent Res. Dev. Sound Vib.* **1**, 29–61.
- Baltanás, J.P., Trueba, J.L. & Sanjuán M.A.F. [2001] “Energy dissipation in a nonlinearly damped Duffing oscillator,” *Physica D* **159**, 22–34.
- Burden, R.L. & Faires, J.D. [1997] *Numerical Analysis*, (ITP, USA).
- Duffing, G. [1918] *Erzwungene Schwingungen bei Veränderlicher Eigenfrequenz* (F. Vieweg u. Sohn, Braunschweig).
- Guckenheimer, J. & Holmes, P.J. [1983] *Nonlinear oscillations, dynamical systems and bifurcations of vectorfields* (Springer, New York).
- Holmes, P.J. [1979] “A nonlinear oscillator with a strange attractor,” *Philos. Trans. Roy. Soc. London A* **292**, 419–448.
- Kapitaniak, T. & Brindley, J. [1998] “Preserving transient chaos”, *Phys. Lett. A* **241**, 41–45.
- Kunze, M. & Küpper, T. [2001] *Nonsmooth dynamical systems: An overview*, in: *Ergodic Theory, Analysis, and Efficient Simulation of Dynamical Systems*, Edited by B. Fiedler (Springer, Berlin-New York) p. 431–452.
- Lima R. & Pettini M., [1985] “Suppression of chaos by resonant parametric perturbations”, *Phys. Rev. A* **41**, 726–733.
- Litak, G., Syta, A., Borowiec, M. [2007] “Suppression of chaos by weak resonant excitations in a non-linear oscillator with a non-symmetric potential”, *Chaos Solitons & Fractals* **32**, 694–701.
- Litak, G., Borowiec, M., Friswell, M.I. & Szabelski, K. [2008] “Chaotic vibration of a quarter-car model excited by the road surface profile”, *Comm. Nonlin. Scien. Numer. Simul.* **13**, 1373–1383.

- Litak, G., Seoane, J.M., Zambrano, S. & Sanjuán, M.A.F. [2012] “Nonlinear response of the mass-spring model with non-smooth stiffness”, *Int. J. Bifur. Chaos* **22**, 1250006.
- Meucci R., Gadomski W., Ciofini M. & Arecchi, F.T. [1994] “Experimental control of chaos by means of weak parametric perturbations,” *Phys. Rev. E* **49**, 2528–2531.
- Melnikov, V.K. [1963] “On the stability of the center for time periodic perturbations,” *Trans. Mosc. Math. Soc.* **12**, 1–57.
- Moon F.C. & Li, G.X. [1985] “Fractal basin boundaries and homoclinic orbits for periodic motion in a two-well potential,” *Phys. Rev. Lett.* **55**, 1439–1443.
- Nusse H.C. & Yorke, J.A. [1997] *Dynamics: Numerical Explorations*, (Springer, New York, USA).
- Ott, E., Grebogi, C., & Yorke, J.A. [1990] “Controlling Chaos” *Phys. Rev. Lett.* **64**, 1196–1199.
- Pavlovskaja, E. & Wiercigroch, M. [2007] “Low-dimensional maps for piecewise smooth oscillators,” *J. Sound Vibr.* **305**, 750–771.
- Qu Z., Hu G., Yang G. & Qin, G. [1995] “Phase Effect in Taming Nonautonomous Chaos by Weak Harmonic Perturbations,” *Phys. Rev. Lett.* **74**, 1736–1739.
- Radons, G. & Neugebauer, R. [2004] *Nonlinear Dynamic Effects of Production Systems*, (Wiley-VCH, Weinheim).
- Robinson, R.C. [2004] *Dynamical Systems: Continuous and Discrete*, (Prentice Hall, London, UK).
- Seoane J. M., Zambrano S., Euzzor S., Meucci R., Arecchi F. T. & Sanjuán, M. A. F. [2008] “Avoiding escapes in open dynamical systems using phase control”, *Phys. Rev. E* **78**, 016205.
- Sprott, J.C. [2003] *Chaos and Time Series Analysis*, (Oxford University Press, New York).
- Verros, G., Natsiavias, S. & Stepan, G. [2000] “Control and dynamics of quarter-car models with dual-rate damping”, *J. Vib. Control* **6**, 1045–1063.
- Von Wagner, U. [2000] “On non-linear stochastic dynamics of quarter car models”, *Int. J. Non-Linear Mech.* **39**, 753–765.
- Zambrano S., Allaria E., Brugioni S., Leyva I., Meucci R. & Sanjuán, M. A. F. [2006] “Numerical and experimental exploration of phase control of chaos,” *Chaos* **16**, 013111.
- Zambrano S., Mariño I. P., Salvadori F., Meucci R., Sanjuán, M. A. F. & Arecchi, F. T. [2006] “Phase control of intermittency in dynamical systems,” *Phys. Rev. E* **74**, 016202.
- Zambrano S., Seoane J. M., Mariño I. P., Sanjuán, M. A. F., Euzzor S., Meucci R., & Arecchi, F. T. [2008] “Phase control of excitable systems,” *New Journal of Physics* **10**, 073030.